اونيۏرسيتي مليسيا ڤهڠ
UNIVERSITI MALAYSIA PAHANG

ORIGINAL ARTICLE

Graphene Nanoplatelets Modified Chemlok® Adhesive System for Natural Rubber – Aluminium Bonded Component in Engine Mount

N.S A. Zulkifli[1], N. Mohamad[1,*], A.A. Abd Ghani[1], S.Y. Chang[1], J. Abd Razak[1], H.E. Ab. Maulod[2], M.F. Hassan[3], M.A.Q. Abu Bakar[3], M.A. Ani[4], M.M. Teng[4] and Q. Ahsan[5]

[1]Fakulti Kejuruteraan Pembuatan, Universiti Teknikal Malaysia Melaka, 76100 Durian Tunggal, Melaka, Malaysia
[2]Fakulti Teknologi Kejuruteraan Mekanikal & Pembuatan, Universiti Teknikal Malaysia Melaka, 76100 Durian Tunggal, Melaka, Malaysia
[3]Kolej Kemahiran Tinggi MARA Masjid Tanah, KM1 Persiaran Paya Lebar, Ramuan China Besar, 78300 Masjid Tanah, Melaka
[4]HML Auto Industries Sdn Bhd, Taman Jati, 45800 Kapar, Selangor
[5]University of Asia Pacific, 74/A, Green Road, Farmgate, Dhaka-1205, Bangladesh

ABSTRACT – Generally, the engine mount is made from rubber and mild steel bonded with a Chemlok® adhesive system. It could be modified to provide sufficient bonding between natural rubber and aluminum. Therefore, this work aims to study a nano-manipulated adhesive system by modifying the existing Chemlok® adhesive system at different weight percentages of graphene nanoplatelets (GNPs) loading via two steps ultrasonic-assisted stirring process by ultrasonic bath and hot plate. The natural rubber (NR)-aluminum (Al) substrates were bonded using a hot press machine under the pressure of 100 kgf/cm2 for 20 minutes at 140 °C temperature. The samples were subjected to a 90-degree peel test based on ASTM D429 by the UTM machine, and the peel-fractured surfaces were evaluated both physically and under SEM. The adhesive strength increased with the increment of GNPs in the modified Chemlok® 205/220 system. The GNPs modified Chemlok® system achieved 30% improvement than the existing adhesive. The analyses proved the modification was successful. The modified system with GNPs dispersed at certain intercalation levels showed active functional groups, reinforcing effects, and thermal stability.

INTRODUCTION

For decades, the rubber-metal combination has created many automotive parts like engine mounts, suspension, and silent blocks to transmit forces and enable defined movements by isolating vibration energy. So, vibrations and noise caused by engine transmission are hardly noticeable [1]. Moreover, in the case of electric engines today, well-adapted engine mounts are needed. Despite coziness, automotive manufacturers are under pressure for better performance like better fuel efficiency and reduction in carbon emissions [2]. Modern automotive demands led to the advancement of rubber-metal generation to enhance wear, impact, and heat. The combination of rubber flexibility and metal stability makes them unique.

Weight reduction is essential since the vehicle trade continues to be dominated by more significant performance and fuel efficiency due to load reduction. But it is challenging to link different materials to form a reliable engine mount system. According to Guadagno et al. [3], structural bonding is not preferable due to the reliability of long-term bonding performance. Previously, rubber with steel bonding had been used in the automobile and aerospace industries. The steel absorbs impact energy in an accident with too much weight compensation and lower corrosion resistance. The engine mount faces incremental demand for lower fuel intake, sound damping, stiffness, and lighter energy efficiency [4]. Therefore, it requires innovative materials and systems. Due to the great importance of the car trade, ensuring a reliable engine mount system always becomes a concern. Therefore, aluminum alloy is replacing steel because of its superior characteristics, such as its lightweight, excellent strength-to-weight ratio, and outstanding mechanical properties to fulfill the performance demands for lightweight vehicles [4].

Automakers prefer a passive bonding system with adhesive joining with the primer coating method. It meets the ease of processing and lightweight principle. Besides, it is simple to maintain, suited to most automotives' demands, and most importantly, cheap. Rubber-based adhesives are commonly used to bond vulcanized rubber to itself and other materials, mainly through a vulcanization bonding [5]. Adhesion occurs when a rubber-based adhesive is introduced between two rubbery polymers. According to Vyoutskii's diffusion theory, the compatibility between the adhesive and substrate is crucial for a strong bond Shybi et al. [6]. Therefore, reinforcing fillers such as carbon-based materials commonly produce strong rubber adhesive. Since these materials are typically used to reinforce rubber vulcanisates, CB is investigated by Shybi et al. [6] in their work. The CB boosts intermolecular or cohesive forces between the connecting surfaces. They have stated that the reinforcing degree is determined by the filler materials' particle size, surface area, and structure. Kardan [7] mentioned that the rubber-based adhesive must have the requisite hardness, mechanical qualities, scorch safety, and cure time. In work by Shybi et al. [6], the peel strengths of the NR-based solution adhesives reinforced by CB

were obtained between 1.9 to 2.0 kg/cm (0.186-0.196 MPa). In comparison, Kardan [7] acquired bonding strength values of around 11 to 22 Ib/in^2 (0.076 -0.152 MPa). Their work compared NR and synthetic NR reinforced with various types of CB.

The superior adhesion between rubber-metal bonding by incorporating carbon black is long utilized in the making of the Chemlok® 205/220 adhesive system. According to Cook et al. [8], the 205 primers comprise chlorinated rubber (most likely chlorinated polyisoprene), epoxy resins, and metal oxides (zinc and titanium). Chlorinated rubbers, carbon black, and a crosslinking agent may be found in the 220 topcoats (adhesive) (sulfur and possibly a dinitroso-containing moiety). Industries widely use it to bond rubber to most metals for many vehicle parts. The utilization of the Chemlok® 205/220 adhesive system is proven to create excellent bonding between rubber with steel and is used widely in engine mount components. It is hypothesized that it could be further modified to provide similar or higher bonding strength for rubber to aluminum.

Yet, the composition of this adhesive system is not publically published. Hence, it is difficult for others to perform any sort of chemical manipulation. Cook et al. [8] had highlighted that manufacturer did not publish the composition of the Chemlok® 205/220 adhesive system. Therefore, nanotechnology would offer an alternative procedure despite focusing on chemical-based modifications that require various chemicals. Quan et al. [9] stated that one way to improve adhesive strength is forming nano-adhesive by reinforcing nanofillers into the adhesive matrix. The graphene nanoplatelets (GNPs) are promising to be compatible nanofillers to enhance Chemlok® bonding strength. This postulate is due to the success findings reported by various researchers while incorporating GNPs into thermoset-based adhesives [9-11] and improvement observed when GNPs were added into rubber materials [12-13]. According to Kuilla et al. [14], nano-functional additives enhance adhesive characteristics. Carbon nanotubes (CNTs) added to epoxy help to improve mechanical properties, thermal conductivity, and long-term durability. GNPs, which are less expensive than carbon nanotubes, have the same effect [14].

Therefore, this research embarks on the potential of incorporating chemically modified GNPs in the Chemlok® 205/220 adhesive system. This research investigates the feasibility of enhancing bonding strength between natural rubber (NR) composites with aluminum (Al) alloy using the modified Chemlok® adhesive system via a vulcanization bonding process. The GNPs loadings of 0, 0.5, 3.0, and 7.0 wt% incorporated into the adhesives were investigated. The postulation is tested against the effect of with and without a Chemlok® 205 primer. The adhesives were prepared via ultrasonication mixing. The NR and Al-alloy sheets were bonded together using a hot press machine at constant parameters and subjected to peel tests using the UTM machine per ASTM D429. Kardan [7] explained the CB reinforcing effect in NR-based adhesives by correlating adhesive strength with infrared (IR) measurements. The IR results show that the reinforcing mechanism promotes trans-conformation. Meanwhile, Shybi et al. [6] supported the peel strength with the thermal characteristics. The CB was observed to increase the thermal stability of the prepared natural rubber-based adhesives. Therefore, in our work, the peel strength of the adhesive systems are explained by both IR and thermal analyses using Fourier Transform Infrared Spectroscopy (FTIR) and Different Scanning Calorimetry (DSC), respectively. Other investigations performed in our research were scanning electron microscopy (SEM), Raman spectroscopy, and x-ray diffraction (XRD).

EXPERIMENTAL METHODOLOGY

Raw Materials and Chemicals

Graphene Nanoplatelets (GNPs) KNG-50 was supplied by Xiamen Graphene Technology Co. Ltd, China. The amounts used in this study were 0, 0.5, 3.0, and 7.0 wt%. The utilized adhesive system was Chemlok® 205 primer and Chemlok® 220 adhesive supplied by HML Auto Industries Sdn Bhd. Meanwhile, ethanol used as the organic solvent was supplied by SystermChemAR. The aluminium 6061-T6 was provided by Fakulti Kejuruteraan Pembuatan, UTeM with a thickness of 1.5 ± 0.05 mm. The aluminum sheet was cut into the desired shape using a laser cutting machine. Meanwhile, the NR60 compound was provided by HML Auto Industries Sdn Bhd.

Preparation of Modified Chemlok Adhesive System

The GNPs were first weighed and divided into four different samples with various loading at 0% (control), 0.5%, 3%, and 7% (Figure 1 and Table 1). It was then kept in a closed bottle to avoid contaminants and spills. The GNPs amount was then dispersed in 25 ml ethanol in an ultrasonic bath for 30 minutes at room temperature. After sonication, the alcohol-treated GNPs were left to dry into powder form overnight in an oven. Then, a specific amount of Chemlok 220 adhesive resin (Table 1) was measured and poured into a beaker before the treated GNPs powder was added. The beaker was then sealed and underwent ultrasonication for 15 minutes. Then, the mixture was transferred onto a hot plate and stirred for another 15 minutes. The mixture formed a stable viscous consistency liquid and was referred to as GNPs modified Chemlok® 220 adhesive and utilized in the subsequent testing and analyses. Then, the structural, compositional, and thermal characteristics of the unmodified Chemlok (control) and GNPs modified Chemlok® 220 adhesives were analyzed. The analyses were performed using x-ray diffraction (XRD), Raman spectroscopy (Raman), Fourier transform infrared spectroscopy (FTIR), and differential scanning calorimetry (DSC). The procedure was to verify the success of the modification process.
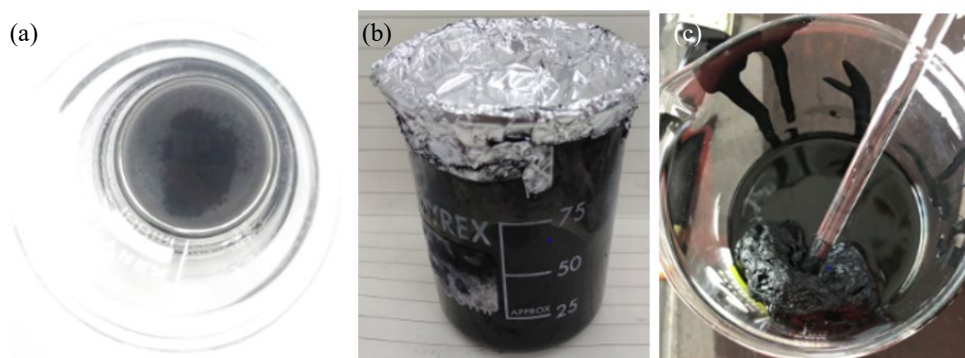
Figure 1. (a) Weighted GNPs in a beaker (b) GNPs dispersed in ethanol and (c) mixture of GNPs and Chemlok® 220.

Table 1. Formulation of control and GNPs modified Chemlok® adhesive systems.

Ingredients/ Sample	Control (0 wt% GNPs)	0.5 wt% GNPs	3.0 wt% GNPs	7.0 wt% GNPs
GNPs (wt%)	0.0	0.5	3.0	7.0
Ethanol (ml)	100	100	100	100
Chemlok® 220 adhesive: Chemlok® 205 primer	3:1	3:1	3:1	3:1

XRD analysis of modified Chemlok system between natural rubber and Al substrate sample performed in the range of 2θ, which 20-70 degrees. This procedure was aimed to identify the presence of phases and their crystallinity level in the adhesive. The Raman analysis was performed using a Raman scattering spectrometer by Uni-Ram 3500 to characterize graphitic and defect bands. The range of Raman shift used to analyze the adhesive film was within 200-2500 cm^{-1}. The FTIR analysis was conducted using a JASCO FTIR-6100 model to identify the functional groups that exist in the adhesive. It was performed at the spectral range of 400 to 4000 cm^{-1} with a resolution of 4 cm^{-1}. The DSC analysis was performed using Perkin– Elmer DSC-7 (United States) analyzer per ASTM E1356 using a sample size of 10 mg; to measure heat energy flow, glass transition temperature (T_g) and melting temperature (T_m) from the DSC thermogram. The analyses were run at a temperature from -50°C to 250°C with a heating rate of 10 °C/min in a nitrogen atmosphere.

Sample Preparation of NR-Al Bonding

After the cutting process, the Al sheet underwent surface cleaning using acetone to clean from debris, oil, and dirt. Then, it was subjected to sandblasting and blew by compressed air to remove the loosely bound sand particles. The substrate surface preparation is a crucial step in leading joint strength. This effect is because a rough surface has higher surface area contact and lets adhesive flow into the irregularities, creating mechanical locking [15-16]. Then, the adhesive systems were applied to the prepared Al sheets according to the scope of the research. A specific brushing method was used for even distribution assurance. A layer of Chemlok® 205 primer was applied to three layers of Chemlok® 220 adhesive ratio on top of the Al sheets (Table 1). For samples without primer, no primer layer was laid before the adhesive.

In the next step, the adhesive-coated Al sheets were inserted in a steel mold cavity with the dimension required for the peel test. Then, pieces of the uncured NR compound were filled into the same cavity to produce samples for peel testing according to the ASTM D429 method B standard. The weight of the NR compound required to fill up the cavity was calculated based on the known volume of the mold cavity and density of the NR compound.

Then the NR-Al is bonded together using a vulcanization bonding technique under a compression load by a hot press machine at 140°C temperature for 20 minutes. The sample was first preheated for 5 minutes before undergoing compression at the pressure of 100 kg-f/cm^2 for 20 minutes to allow both adhesive and NR to cure simultaneously. After that, it was left to cool down for 5 minutes. After conditioning for 24 hours, the samples were subjected to a 90-degree peel test according to the ASTM D429-Method B standard using a 20 kN UTM machine.

Testing and Analyses of NR-Al Bonding

The mechanical performance of the adhesive bonding was determined by the Universal Testing Machine of 20kN capacity, as in Figure 2(a). The samples were subjected to a peel test to characterize the properties of NR-Al bonded with both unmodified and modified Chemlok® 220 adhesive. Method B of ASTM D429 was chosen to test rubber on metal substrate adherence by performing a 90° peel strip test.

According to ASTM D429, the sample dimension recommended was 6.3 mm thick, 25 mm wide, and 125 mm long. At the same time, the aluminum substrate had a thickness of 1.6mm, 25mm wide, and 60 mm long, and the bonded area was 25×25 mm at the center of the metal specimen. A 50 mm/min testing speed was used until rubber separated from the metal substrate. A constant rate of machine head travels at 0.83 to 0.08 mm/s following ASTM D429. Figure 3(a) and 3(b) show the peeling test and flat peel test fixture to carry out the testing. The maximum force and maximum stress were calculated to evaluate the energy release rate used to split NR and Al substrate.
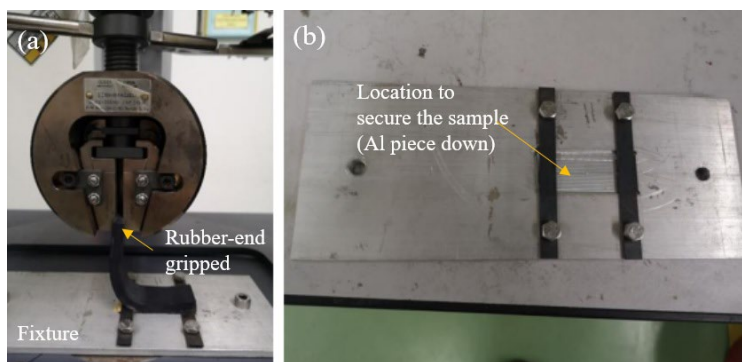
Figure 2. (a) 90° peeling test and (b) flat peel test fixture.

After the peel test was conducted, the peel-fractured NR-Al surfaces were collected and analyzed. It is to study the correlation between fracture morphology with the effects of GNPs loadings and the presence of Chemlok® 205 primer. Samples that had given peel strength values closed to the average were selected for failure surface analyses. The type of failure mode could trace the type of adhesion formerly formed between NR and Al sheets. The physical criteria of the surfaces were analyzed under optical microscopy to identify the failure mode, either adhesive or cohesive failure. The morphological characteristics were examined using scanning electron microscopy (SEM) analyses.

RESULTS AND DISCUSSION

XRD Analysis of GNPs Modified Chemlok 220 Adhesives

Figure 3 shows XRD diffractograms of samples at 0, 0.5, 3.0, and 7.0 wt% GNPs that exhibit similar patterns in every composition. It represents almost sharp narrow peaks at $\sim 2\theta = 26.47°$ at various formulations regardless of the GNPs loadings. However, peaks intensity decreased with GNPs content. These signals indicate that the adhesive systems are composed of highly crystalline materials. The characteristic peak for the main crystalline graphitic structure was reported at $2\theta = 26.5°$ [17]. The peak corresponds to the interlayer spacing of 3.34Å. Besides, it is clearly observed in Figure 3 that unmodified Chemlok® adhesive already shows a higher peak at $2\theta = 26.47°$. The unknown composition of the original Chemlok® adhesive itself may contain other crystalline carbon-based elements such as carbon black (known to be aggregated at nanoscales level) [18]. According to Cook et al. [8], carbon black particles are one of the ingredients in the Chemlok 220 adhesive.
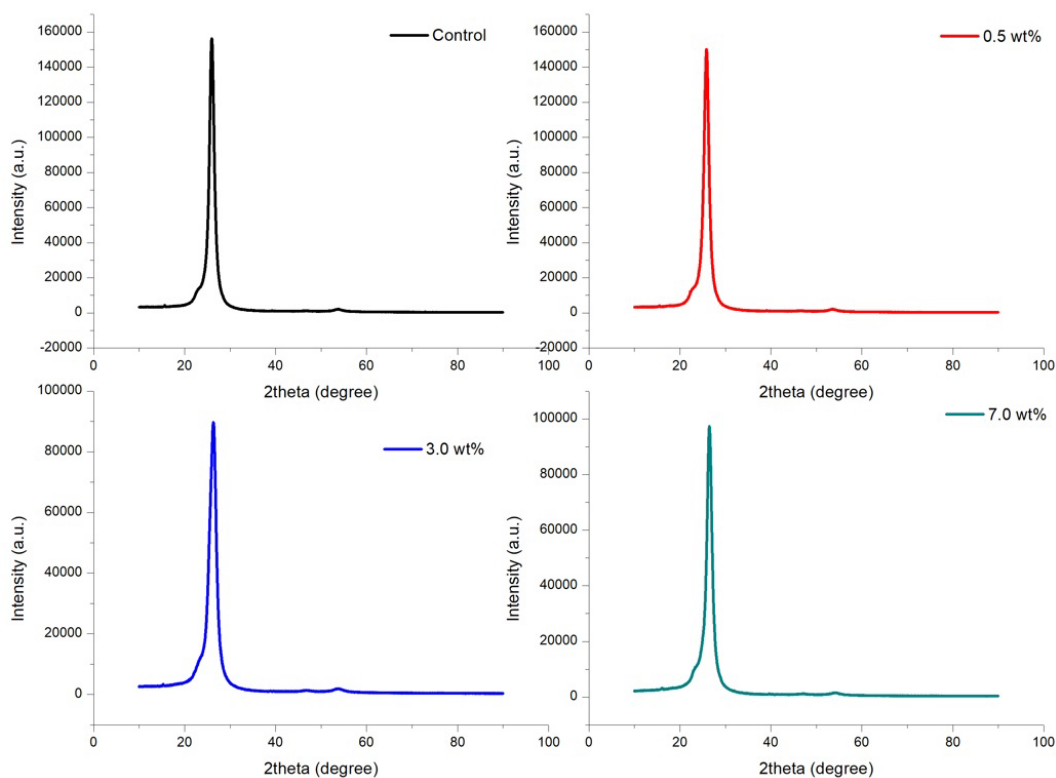
Figure 3. XRD spectra of unmodified and GNPs modified Chemlok® 220 at 0, 0.5, 3, and 7 wt%.

This study observed a pronounced reduction when more GNPs were added into Chemlok® 220 adhesive. The degree of crystallinity was reduced after GNPs loadings, as indicated by the decrease of peak intensity in all GNPs modified systems compared to the control sample. The decrement could be due to either higher 1) phase separations or 2) intercalations of GNPs platelets that had been taken place in adhesive systems. The disappearance of GNPs characteristics peaks of around 10 (2θ) from the XRD spectra in some nanocomposites was also reported. The changes indicate that the nanoplatelets are uniformly dispersed within the matrix [1, 19].

At the shoulder of 002 peaks at ~2θ = 23.4°, all adhesives show a slight swelling, indicating amorphous structures. The broadening appears slightly more prominent at the 3.0 wt% GNPs loading. The small broadening peaks indicate slight amorphous structures in the Chemlok® adhesive system. The rising of GNPs in control Chemlok® introduced significant interactions that altered the materials structure and crosslinking criteria [20]. The newly formed structure could be due to the intercalation effect of GNPs with polymeric adhesive chains. It corresponds to a higher degree of amorphous and disordered structure in the nanocomposites. Still, there could be overlapping signals between GNPs and the existing crystalline carbon materials in the adhesive, probably carbon black with the adhesive matrix. Almost identical results were obtained by Ahmadi et al. [1]. The XRD diffractogram of epoxy nanocomposites filled with GNPs showed a small blurry peak at 2θ=26.6°. This peak signifies the presence of an epoxy polymer matrix. Meanwhile, Alhumade et al. [19] found that the XRD pattern showed a broadening peak appearing at a 2θ value in the range of 10 to 30°. The observation was reported to belong to homogeneously amorphous epoxy nanocomposites.

Raman Analysis of GNPs modified Chemlok 220 Adhesives

Figure 4 shows D and G peaks from Raman spectra for unmodified Chemlok® 220 adhesive (control sample) and the GNPs modified Chemlok 220 adhesives at different GNPs loading. From the figure, there are two strong visible signals, D and G bands at 1410 cm^{-1} and 1620 cm^{-1}, corresponding to graphitic carbon materials, and they are in good agreement with the one reported by Yoo et al. [21]. The intensity of the D band signifies the degree of defects in adhesive due to other compositional elements in both systems. The D band indicated breathing mode of κ-phonons of A1g symmetry, while the G band ascribed to the first-order scattering of E2g phonons.
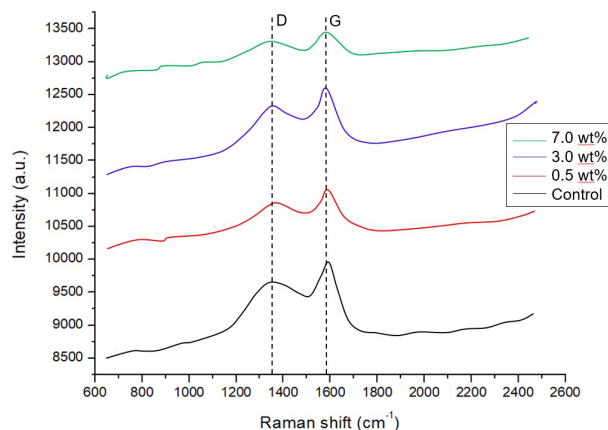
Figure 4. Raman spectra of unmodified and GNPs modified Chemlok® 220 systems.

Table 2 tabulates the ID/IG ratio of both unmodified and GNPs modified adhesive. All samples show Raman spectra having similar wavenumber positions except for their intensity. The presence of carbon black in the 220 topcoats would be the reason for this observation [8]. Therefore, the GNPs and carbon black's contribution to the structural difference could have been overlapped. Furthermore, it might also be due to the possible agglomeration and surface properties of GNPs in the adhesive. The difference in intensity depicts the level of disorders in their carbon-based material. The ratio value lower than one means defect level in the adhesive system is high but still acceptable; lower ID than IG values.

Table 2. Raw data result of D peak and G peak.

Samples	D peak	G peak	ID/IG ratio
Control (0 wt% GNPs)	1410.307 a.u.	1622.673 a.u.	0.8691
0.5 wt% GNPs	1410.648 a.u.	1623.219 a.u.	0.8690
3.0 wt% GNPs	1410.632 a.u.	1617.076 a.u.	0.8723
7.0 wt% GNPs	1407.140 a.u.	1619.930 a.u.	0.8686

The ratio gradually increased with the increasing carbon content in most reported carbon nanomaterials' reinforced polymer composites [22]. However, a slight reduction of ID/IG ratio was observed in this study except at the GNP loading of 3.0wt%. The decrease of ID/IG ratio when GNPs at 0.5 wt% indicated an improved GNPs dispersion in the adhesive. Whereas, as the amount was added at 3 wt%, the dispersion dropped due to the agglomeration effect [23]. The area ratio of the D band to G band (ID/IG) between carbon atoms with sp2 and sp3 hybridization in the graphitic lattice indicates the degree of oxidation. The excellent value is 0.106 by estimation [24]. According to Song et al. [24], the lower ID/IG area ratio showed fewer impurities and defects in GNP structure, leading to the high thermal conductivity of GNP. The

incorporation of GNPs into Chemlok® adhesive systems at the only low amount is observed to favor the dispersion of GNPs in intercalation structures which then reduced the ID/IG ratio. Despite the worsened agglomeration of GNPs at 7 wt%, in the form of graphite [25], the ID/IG ratio was reduced. It would result from existing hydroxyl groups on the GNPs surface, more pronounced at a high loading of 7 wt%. Their presence reduces the defect sites of the GNPs.

FTIR Analysis of GNPs Modified Chemlok 220 Adhesives

The FTIR analysis was conducted to identify the adhesive systems' functional group and molecular components by comparing its' characteristics signals from existing chemical groups and additives [26]. The data was interpreted and analyzed by comparing the established IR spectra for a chlorinated polyisoprene system (the based system for Chemlok 220 adhesive). The FTIR analyses for both unmodified Chemlok 220 adhesive (control sample) and GNPs modified Chemlok 220 adhesive at different GNPs loadings were carried out against the reported FTIR spectra by Jiang et al. (2017)[26]. Their work was on the viscoelastic behavior of chlorinated butyl rubber reinforced with graphene oxide.

The spectra of the adhesives system in this study are depicted in Figure 5. It is observed that IR spectra for Chemlok adhesive resemble the IR spectra of chlorinated rubber reinforced by graphene oxide, as reported by Jiang et a.[26]. Spectra in Figure 5 depicts the characteristics peaks for chlorinated rubber. At 650 cm^{-1}, the band represents the stretching vibration of C–Cl, probably from chlorinated rubber [18]. Peaks at around 3400–3600 and 1439 cm^{-1} correspond to O–H's deformation vibration. The bands at around 2800 and 2900 cm^{-1} agree with Kardan [7]. They correspond to the stretching vibration of methylene groups by C–H bonds. Kardan [7] studied the potential of CB reinforced NR and SNR composites for adhesives and sealants. The IR bands at the 2970 cm^{-1} and 2870 cm^{-1} regions can be assigned to asymmetric and symmetric stretching vibrations of CH_3 groups. Meanwhile, the bands at 2928 and 2858 cm^{-1} correspond to the asymmetric and symmetric stretching vibrations of methylene (CH_2) groups.
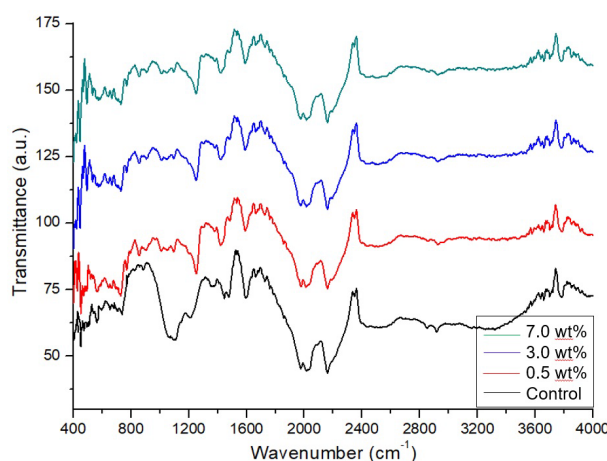
Figure 5. FTIR spectra of modified Chemlok at varies GNP wt%.

The IR bands between 1100 to 1200 cm^{-1} could be registered to the stretching vibrations of C–O. According to Jiang et al. [26] the bands at 1115 and 1121 cm^{-1} originate from the C–O stretching vibrations. Meanwhile, the 1620 and 1625 cm^{-1} bands correlate to the stretching vibration of C=O. Additionally, the broad peak around 3400 cm^{-1} and the peaks near 1399 cm^{-1} could correspond to the O–H deformation vibration. These functional groups could be the contributions from the presence of GNPs and probably the carbon black. When GNPs were added, more noticeable peaks at between 1200 and 1300 cm^{-1} were observed. By and large, the shift in wavenumber is ascribed to physical interaction (hydrogen bond, etc.). Additionally, no other distinctive peaks are noticed when GNPs are introduced into the Chemlok system. As a result, the interaction between GNPs and the system can be mainly attributed to physical interaction.

In Figure 5, FTIR spectra of all adhesive systems incorporating GNPs show almost identical functional groups. Meanwhile, for the control sample without GNPs, apparent differences were observed in the IR absorption range of 600 to 1400 cm-1. GNPs in the adhesives produced overlapping peaks with chlorinated rubber at ~2300 cm^{-1}. According to Gunasekaran et al. [27], C-H symmetrical stretching and double bond stretching of the methylene group may be observed in GNPs having a characteristic peak at ~2361 cm^{-1}. Yet, increment of GNPs in Chemlok adhesive systems was observed to show identical and stronger IR signal strength than the unmodified Chemlok. Many swelling peaks were observed in the unmodified Chemlok. It depicts the complexity of formulation and solvent present in the system. The identical IR spectra of GNPs modified Chemlok adhesives show the consistent interaction in the system with the incorporation of GNPs.

DSC Analysis of GNPs Modified Chemlok 220 Adhesives

The DSC thermogram is utilized to identify glass transition temperature, T_g, and melting point, T_m, which show thermal stability and conductivity of Chemlok® adhesive. Figure 6 shows DSC thermograms for unmodified and GNPs modified Chemlok® adhesive at 7.0wt% GNPs loading having almost similar patterns showing melting point and glass transition temperature.

It is well noted that both T_g and T_m rise with the incorporation of GNPs in Chemlok® adhesive from Table 3. The increment of T_g indirectly reflects the increment in the reinforcing effect of filler material (discrete phases) to matrix material (continuous phase) of the adhesive system. Similar results were reported by Quan et al. [9] and Xue et al. [28]. In addition, T_g is the attribution of polymer segmental mobility. The nanoparticle loading in polymer matrices leads to a rise in T_g due to homogeneous dispersion [1]. The addition of GNPs at 7 wt% to the adhesive eventually still provides an appreciable reinforcing effect to the polymeric adhesive matrix, despite the agglomeration.

In contrast, T_m signifies the heat energy required for materials to melt. It shows the stability of the cured adhesive system under the influence of elevated temperature. It is observed that GNPs modified adhesive system need a higher temperature to transform to molten state due to the GNPs efficiency as heat conductivity channels to dissipate heat from adhesives while subjected to heating, as reported by Li et al. [29]. The applied heat from the DSC system is absorbed by GNPs and heat transferred out from modified Chemlok® adhesive, hence prolonging the system's life from thermal degradation. So, it is clear that the thermal properties of cured modified Chemlok® adhesives were observed to improve with the incorporation of GNPs.
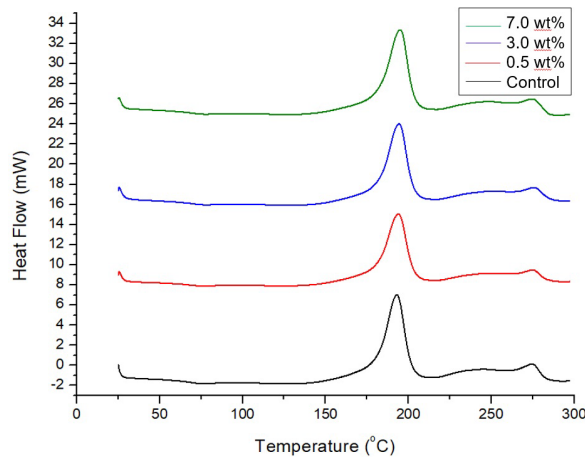
Figure 6. DSC thermogram of unmodified Chemlok® 220 (control) and GNPs modified Chemlok® 220.

Table 3. Comparisons of Tg and Tm for unmodified and modified Chemlok adhesives.

Temperatures (°C)	Unmodified Chemlok (0 wt% GNPs)	Modified Chemlok (7 wt% GNPs)	Temperature difference (°C)
Glass transition, Tg			0.97
Melting temperature, Tm	67.95	68.92	1.97

Peel Strength of GNPs Modified Chemlok 220 Adhesives

Figure 7 shows the average maximum stress (peel strength) for NR-Al bonded with modified Chemlok® 220 adhesive samples calculated from the number of samples, n of equals to 7. The comparison is made for the effect of with or without primer and the GNPs loading. The highest performance under the peel test observed in the modified Chemlok® at 3 wt.% GNPs without primer has the average maximum peel strength of 0.186 MPa. The data manifests a similar pattern where peel strength increases when GNPs loading increases to 3wt% and drops once it reaches 7wt%. This could be due to agglomerations when more GNPs added to Chemlok® adhesive. It is in good agreement with the morphological characteristics of the NR-Al peel-fractured surfaces.

Adhesive system	Peel Strength (N/mm²)			
	GNPs loading (wt%)			
	0	0.50	3.0	7.0
Without Chemlok® 205	0.11	0.148	0.186	0.136
With Chemlok® 205	0.173	0.219	0.186	0.136
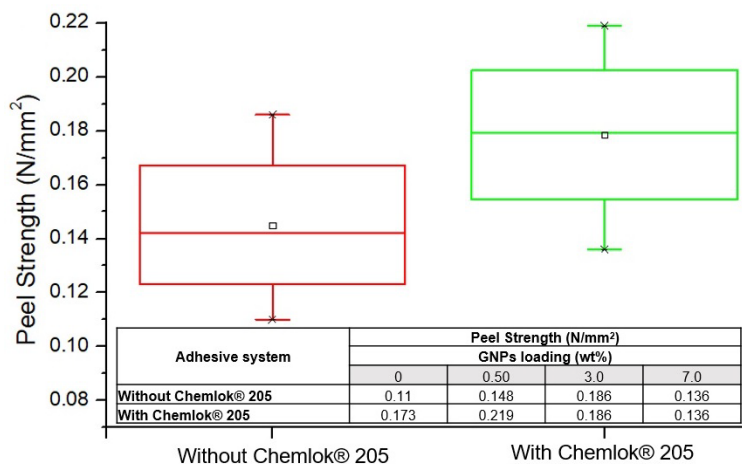
Figure 7. Comparison of peel strength between adhesive systems without and with the utilization of Chemlok® 205 (n = 7).

The lowest peel strength value observed in NR-Al bonded with the modified Chemlok 220 adhesive loaded with GNPs at 7wt% with primer. In contrast, the highest performance was exhibited by modified Chemlok 220 adhesive loaded with GNPs at 0.5wt%. The average maximum peel strength is 0.219 N/mm^2 (MPa) at a minimal standard deviation of 0.04636. The obtained value is even higher than the maximum strength obtained by [6-7]. It shows that the reinforcing effect was higher at lower GNPs loading in modified Chemlok® adhesive due to the ease in GNPs dispersion. According to Chong et al. [30], good dispersion and dispersion are crucial to achieving the best balance of materials' properties. The presence of hydroxyl on the GNPs could also contribute significantly to the bonding strength of the Al - rubber interface. Gong et al. [5] has stated the positive role of the hydroxyl groups towards bonding strength, in their work.

The maximum peel strength is considered the determination point for the bonding strength of the systems. It is noted that GNPs facilitate to improve strength for Chemlok® 220 but have a negative interaction with Chemlok® 205 primer once used together at a high amount. Therefore, it is deduced that the optimum amount of GNPs loading in the system could be between 0.5wt% to 3wt%.

Beyond 3.0wt%, GNPs loadings were shown to give trivial effect to the improvement of Chemlok® adhesive since both samples without primer and samples with Chemlok® 205 primer have the same average peel strength 0.186 N/mm^2 and 0.136 N/mm^2, respectively. The observation proves the importance of the GNPs dispersion effect and the agglomeration issues at high GNPs loading. At a high loading of more than 3.0wt%, GNPs particles have hardly been dispersed throughout the Chemlok® 220 matrix. The agglomerates imposed extra resistance (torque) to the stirring process. Furthermore, it reduces GNPs dispersion and distribution homogeneity in the Chemlok® adhesive matrix [9].

Failure Mode Analysis of NR-Al Peel-Fractured Surfaces

Table 4 lists the failure surface of both Al and NR for NR-Al bonded with unmodified and GNPs modified Chemlok® 220 adhesive. In all samples conditions, their peel-fractured surfaces manifest the appearance of both adhesive and cohesive failure. So, fracture mode for the system is a combined adhesive-cohesive failure depending on the amount of GNPs and the presence of Chemlok 205 primer in the NR-Al bonding system.

The trace area of rubber material presence on top of the Al sheet and the degree of irregularity is used to deduce the cohesivity/ adhesive bonding level. A fracture surface, where many adherent materials stick to another adherent surface, is considered to experience cohesive failure. Samples manifesting these fracture criteria have the possibility to show a high bonding strength.

It is well noted from Table 5 that NR-Al bonded with modified Chemlok adhesive at 3wt% GNPs loading and 0.5wt% showed the highest cohesivity degree for the system without and with primer, respectively. The highest peel strength of 0.225 N/mm^2 by 0.5 wt% sample with primer has a rough surface for both adherent due to cohesion failure. Among all eight samples, the lowest peel strength of 0.115 N/mm^2 was achieved by the sample at GNPs loading of 7wt% without primer. The Al fractured surface for this sample appears clean with slight traces of adhesive or rubber. The peel-off surface at the adhesive layer is identified as an adhesive failure.

Cohesive failure happens in the bulk adhesive layer or the bulk of adherents. The adhesive failure occurs in the interfacial surface between adhesive and adherent. The cohesive failure is preferable failure mode as high fracture toughness is vital in maintaining adhesive joint stability. The peel strength enhancement in the GNPs modified Chemlok® 220 adhesive could be attributed to the improved interaction between GNPs and Chemlok matrix that facilitates crack bridging and deviation. Ahmadi [31] stated that the fracture mechanism in composite depends on interfacial strength between nanoparticles and matrix and nanoparticles flexibility. Aside from interaction between GNPs and Chemlok® matrix, primer is vital in boosting cohesive failures in bonding. It is observed in Table 4 that NR-Al peel-fractured surfaces for the system with primer showed a higher degree of cohesive failure. Cohesive failure mode was dominant in samples with the highest peel strength [32]. The primer eases the mobility of filler and enables more uniform distribution of filler in adhesive during vulcanization.

SEM Observations

From the failure mode analysis, it is agreed that the rougher surface of the adherent indicates the cohesive failure, which proved the excellent bonding strength between adhesive and adherent [32]. Figure 8 shows the peel-fractured surface of both NR and Al surface bonded by unmodified Chemlok® 220 adhesive without incorporating GNPs at 50× and 500× magnifications. Both Figure 8(a) and Figure 8(b) show the shear yielding mechanism of the adhesive on top of the Al substrate. It offers a relatively smoother surface with shorter fibrils from the effect of brittle-like failures of adhesive. While, NR surface at 50× magnification in Figure 8(c) exhibits two different regions; area A is the peeled-out NR adherent, and area B is the adhered adhesive on the NR surface. The fractured surface of the adhesive layer occurred at ~90∘ angles from the NR substrate. This characteristic indicates the adhesive to fail in brittle-like failure. However, the NR surface fracture showed a significant bond between the adhesive and adherents. The adhesive layer could be estimated from the slanting surface of the adhesive ripped out from the NR substrate and was estimated to be ~35 µm thickness.

The fracture surfaces on the NR substrate show a relatively rougher morphology than those on the aluminum substrate by comparing Figure 8(b) and Figure 8(d). This is because the adhesive-bonded with rubber adherent is more significant than the metal substrate. During peel test, adhesive and rubber experienced a more pronounced plastic deformation from the difference in molecular flexibility; aluminum is a far stiffer material than NR or adhesive.

Figure 9 shows the peel-fractured surfaces of both NR and Al for the system, which obtained the highest peel strength; the one bonded with modified Chemlok® 220 adhesive at the GNPs loading 0.5wt% with the presence of primer. It is evident that both surfaces show high surface roughness and irregularities. From Figure 9(a), a high degree of fibrillation

occurred to the adhesive that adhered to the Al substrate. This is due to the shear yielding mechanism due to the difficulty of tearing during the peeling process. This sample required more energy and forces to break bond interaction between the interfaces of two adherents; NR and Al surfaces. This characteristic corresponds to a higher degree of GNPs modified Chemlok® adhesive ductility. Liang et al. [33] reported that good GP dispersion of GPs in the Chemlok® adhesive system via stirring had increased the bonding strength. This argument is supported with the fracture surface on NR substrate in Figure 9(b), where the adhered adhesive has a radial fracture at an angle of less than 45∘.

By analyzing Figure 9(b) and 9(c), it could be deduced that adhesive had bonded strongly to both NR and Al surfaces. There are portions of adhesive that adhered to the surface of NR in Figure 9(b) hence validating the portion of missing adhesive in Table 4. The adhesive layer could be estimated from the slanting surface of the adhesive ripped out from the NR substrate in Figure 9(c) and estimated to be ~35 μm thickness. The adhesive appeared on the NR surface, and the magnified morphology is depicted in Figure 9(d). The surface of the adhered adhesive on NR seems to be more brittle-like, with a smoother texture from the shear yielding mechanism.

Table 4. Failure surfaces of NR and Al after peel testing.

Sample	Has primer	No primer
Control (0 wt% GNPs)	Peel strength= 0.103N/mm²	Peel strength= 0.172N/mm²
0.5 wt% GNPs	Peel strength= 0.152N/mm²	Peel strength= 0.225N/mm²
3.0 wt% GNPs	Peel strength= 0.182N/mm²	Peel strength= 0.190N/mm²
7.0 wt% GNPs	Peel strength= 0.115N/mm²	Peel strength= 0.120N/mm²
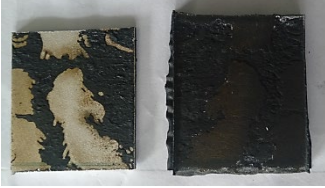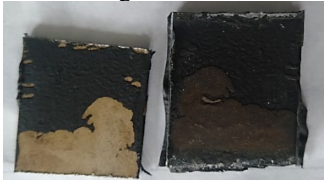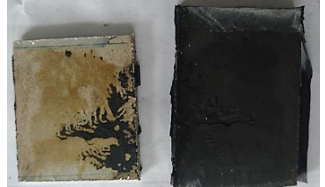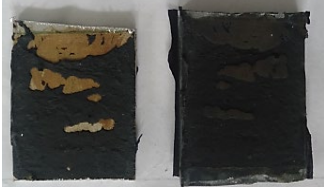
As stated, the NR-Al samples that bonded with the unmodified Chemlok® adhesive without primer had the lowest peel strength of 0.110 MPa. Figure 8 generally represents the weakest adhesive bonding of the Chemlok® adhesive system. While SEM observation in Figure 9 for NR-Al sample bonded with modified Chemlok adhesive at GNPs of 0.5wt% system with the presence of primer represents the system with the most vital bonding strength. The average maximum peel strength of the system was 0.219 MPa. By comparing Figure 8 and Figure 9, the system with the strongest bonding appeared to have higher surface roughness, adhesive ripping angle of less than 45∘ with a higher degree of plastic yielding mechanism corresponding to higher energy required to break the bond between adhesive and adherents.

Figure 10 compares SEM micrographs of peel-fractured surfaces for unmodified Chemlok® and GNPs modified Chemlok® adhesives on Al sheets. It is evident from the images that modified Chemlok® showed higher surface roughness with a higher degree of shear yielding mechanism than unmodified Chemlok. From the slight brighter contrast, the presence of GNPs spotted. In Figure 10, GNPs are seen to be located at thick tearing lines of yielded polymers. This argument is supported further with the micrographs in Figure 11 on both Al and NR substrates. The crack face area is filled with plate-like materials with lighter contrast pointing out GNPs. This criterion shows that the GNPs were bridging the crack face and increasing the stress to fracture.
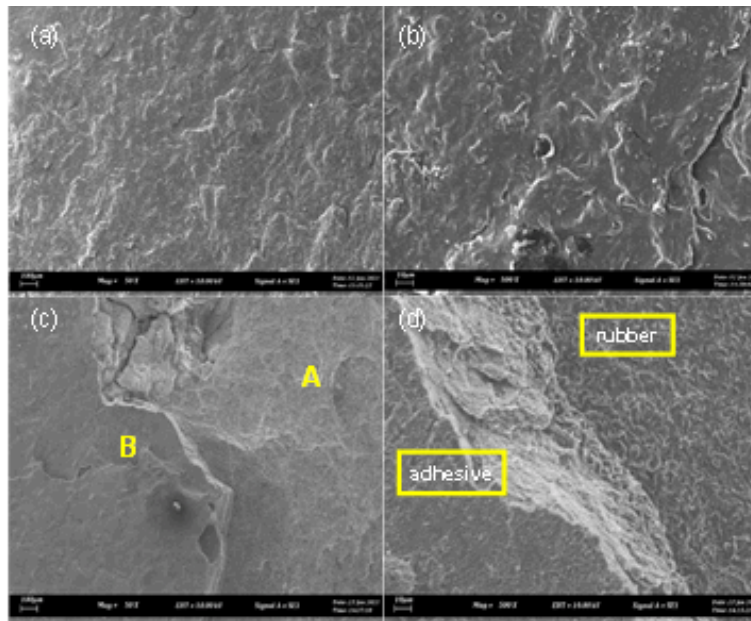
Figure 8. SEM micrographs of NR-Al peel-fractured surfaces bonded with neat Chemlok® adhesive at 0 wt% GNPs for (a) Al surface at 50× magnifications, (b) Al surface at 500x, (c) NR surface at 50× magnifications, and (d) NR surface at 500× magnifications.
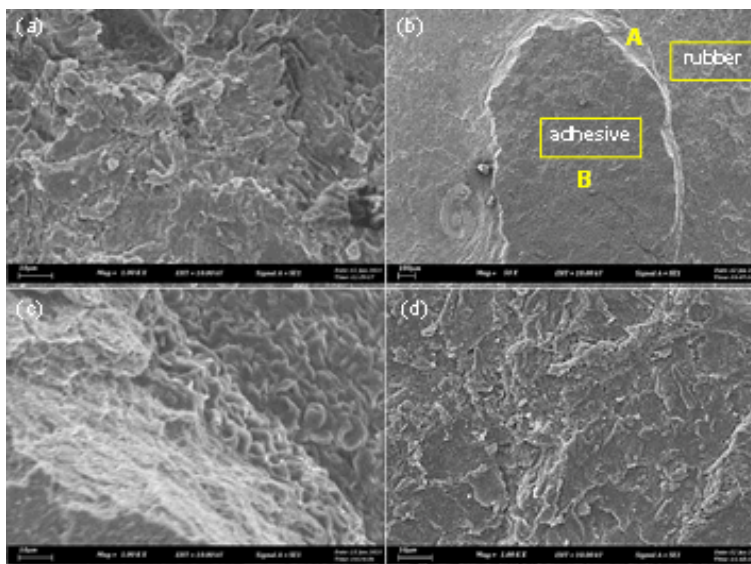
Figure 9. SEM micrographs of NR-Al peel-fractured surfaces bonded with modified Chemlok® adhesive at 0.5 wt% GNPs for (a) Al surface at 500× magnifications, (b) NR surface at 50× magnifications, (c) NR surface (A area), and (d) adhesive on NR (B area) at 500× magnifications.
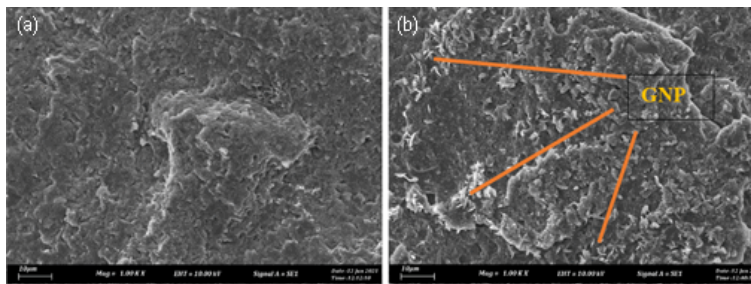
Figure 10. SEM micrograph of (a) unmodified Chemlok® and (b) modified Chemlok® at 3.0 wt% GNP loading on Al substrates 1000× magnifications.

Figure 12 compares SEM images for the effect of modified Chemlok® 220 adhesives for 0.5, 3.0, and 7.0wt% GNPs loading on Al surfaces. The surface irregularities increase with GNPs loading in the Chemlok® matrix. The evaluation

of peel strength for the effect of filler loading stated that the peel strength for NR-Al bond primer presence varied from 0.219 N/mm², 0.186 N/mm² to 0.136 N/mm² from the one filled with 0.5 wt%, 3.0 wt%, and 7.0 wt%, respectively.
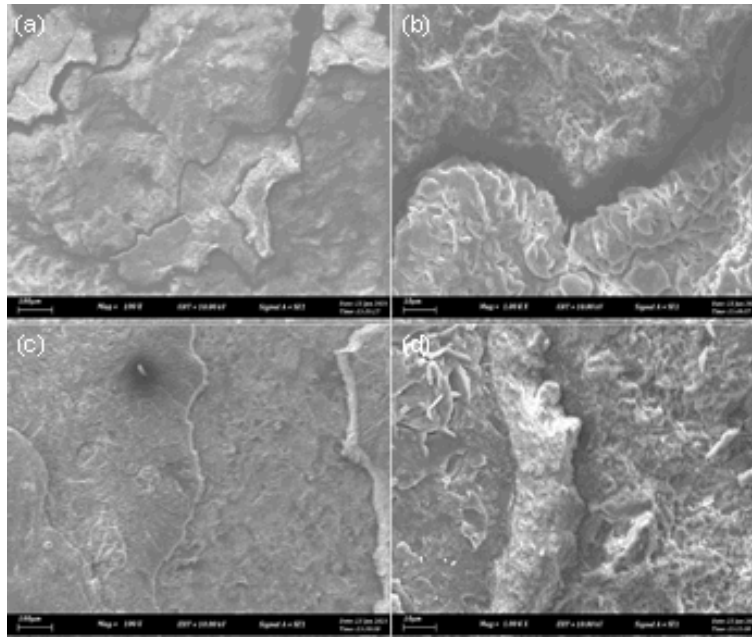
Figure 11. SEM micrographs of NR-Al peel-fractured surfaces bonded with modified Chemlok® adhesive at 0.5 wt% GNPs for (a) Al surface at 100× magnifications, (b) Al surface at 1000× magnifications, (c) NR surface at 100× magnifications, and (d) NR surface at 1000× magnifications.

From Figure 12, the qualitative increment in surface roughness due to the clustering of GNPs particles turning into larger particles became a stress concentrator factor that reduces the bonding strength of the adhesive phase. Voids formations in modified Chemlok® 220 adhesives filled with 7.0 wt% (as in Figure 13). The increase in viscosity of the adhesive matrix at higher GNP loadings had restricted the adhesive flow to fill up space between adherents during vulcanization curing. The viscous adhesive body could trap the vaporized chemicals formed during the vulcanization process. Then, it remained as voids which reduced the surface adherence and lowered the bonding strength of the NR-Al bond. The wettability of adhesive decreases with GNPs loading in modified Chemlok® 220 adhesive. The observations are in line with the bonding strength of NR-Al bonded with modified Chemlok® 220 adhesive.
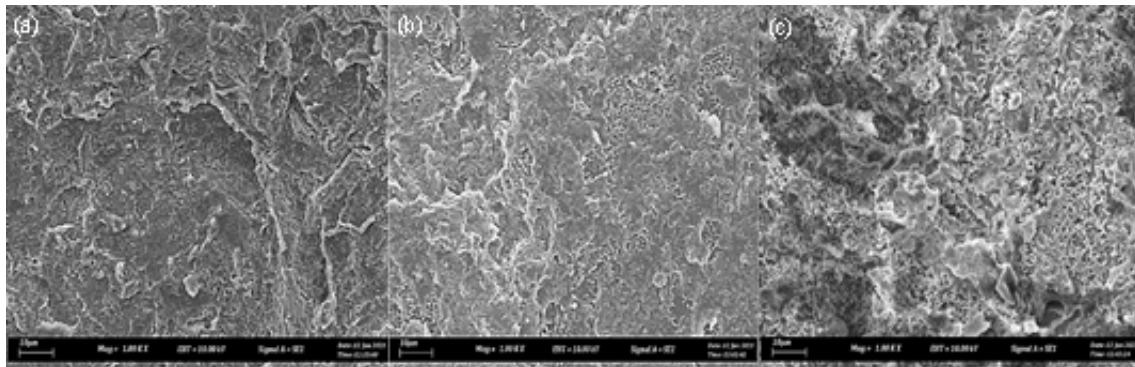
Figure 12. SEM micrograph of modified Chemlok® 220 adhesives at (a) 0.5 wt%, (b) 3.0 wt% and (c) 7.0 wt% GNPs loadings (1000× magnifications).
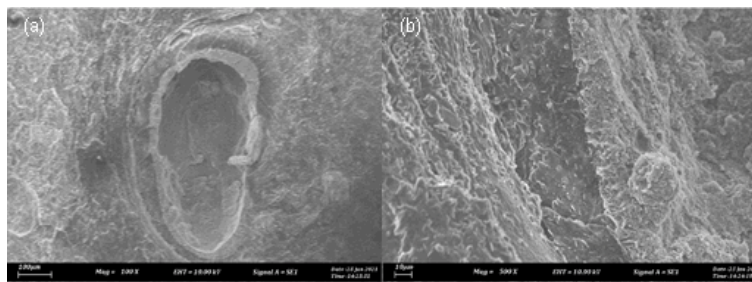
Figure 13. SEM micrographs of void formation on NR substrates at (a) 100× magnifications and (b) 1000× magnifications for the modified Chemlok® adhesive system.

CONCLUSION

This study modifies Chemlok® 220 adhesive by incorporating graphene nanoplatelets (GNPs) at 0.5, 3.0, and 7.0 wt% with and without Chemlok® 205 primer. The GNPs modified Chemlok® was successfully prepared and analyzed for structural, compositional, and thermal characteristics using XRD, Raman, FTIR, and DSC, respectively. The peel strength of NR-Al bonded with GNPs modified Chemlok 220 adhesive increases with increasing GNPs loading at certain optimum loading content. The percolation threshold of 3.0 wt% was achieved for GNPs modified Chemlok® system without primer. In contrast, the system with primer exhibited a percolation threshold at 0.5 wt% GNPs loading. The optimum GNPs loading to modify Chemlok® 220 adhesive system lies in between 0.5 to 3.0 wt% GNPs loading. Improvement of GNPs dispersion level in Chemlok adhesive could further improve the bonding strength of NR-Al bond. The improvement in peel strength for the effect of suitable GNPs loading with primer in a modified adhesive system is ~30%. All of the fracture surfaces showed a combination of adhesive and cohesive failures mode. The NR-Al peel-fractured surface bonded with adhesive at 0.5 wt% GNPs loading with primer had the widest area of cohesive failure. The results were supported by fracture surfaces' characterization using the SEM analyses. The finding is expected to contribute to the local automotive industries and relevant industries that utilize metal to rubber bonding components.

ACKNOWLEDGEMENT

REFERENCES

[1]   B. Ahmadi, M.Sharafimasooleh, S. Shadlou, and F. Taheri, "Effect of functionalization of graphene nanoplatelets on the mechanical response of graphene/epoxy composites," *Mater. Des.*, vol. 66, pp. 142-149, 2015, doi: 10.1016/j.matdes.2014.10.047.

[2]   M. A. Fentahun, and M.A. Savas, "Materials used in automotive manufacture and material selection using Ashby charts," *Int. J. Mater. Eng.*, vol. 8, no. 3, pp. 40-54, 2018, doi: 10.5923/j.ijme.20180803.02.

[3]   L. Guadagno, M. Sarno, C. Cirillo, and P. Ciambelli, "Graphene-based structural adhesive to enhance adhesion performance," *RSC Adv.*, vol. 5, no. 35, pp. 27874-27886, 2015, doi: 10.1039/C5RA00819K.

[4]   T. Ramachandran, S. Surendarnath, and R. Dharmalingam, "Structural and suitability analysis of aluminium metal matrix composites for IC engine mountings," in *Materials Today: Proceedings*, vol. 37, no. 2, 2021, pp. 1524-1528, doi: 10.1016/j.matpr.2020.07.145.

[5]   N. Gong *et al.*, "Effect of metal surface state on injection joining strength of aluminum-rubber composite part," *J. Manuf. Proccess.*, vol. 49, pp. 365-372, 2020, doi: 10.1016/j.jmapro.2019.12.006.

[6]   A.A. Shybi, S.Varghese, V. Nambiathodi, and S. Thomas, "Natural rubber-based solution adhesives: effect of carbon black on the adhesive properties," *J. Rubber Res.*, vol. 24, pp. 187–196, 2021, doi: 10.1007/s42464-021-00084-w.

[7]   M. Kardan, "Carbon black reinforcement in natural rubber-based adhesives and sealants," *Int. Poly. Sci. Technol.*, vol. 31, no. 1, pp. 7-10, 2004, doi: 10.1177/0307174X0403100102.

[8]   J.W. Cook, S. Edge, and D. E. Packham, "Bonding of natural rubber to steel: surface roughness and interlayer structure," *The J. Adhes.*, vol. 72, no. 3-4, pp. 293-315, 2000, doi: 10.1080/00218460008029287.

[9]   D. Quan *et al.*, "Mechanical and fracture properties of epoxy adhesives modified with graphene nanoplatelets and rubber particles," *Inter. J. Adhe. Adhes.*, vol. 81, pp. 21-29., 2018, doi: 10.1016/j.ijadhadh.2017.09.003.

[10]   S. Remanan, T.K. Das, and N.C. Das, "Graphene as a reinforcement in thermoset resins," in *Polymer Nanocomposites Containing Graphene Preparation, Properties, and Applications*, M. Rahaman, L. Nayak, I.A. Hussein, and N.C. Das, Eds. Woodhead Publishing Series in Composites Science and Engineering, pp. 317-341, 2022, doi: 10.1016/C2019-0-04352-X.

[11]   Z.-J. Li *et al.*, "Flexible epoxy graphene thermoset with excellent weather and corrosion resistance," *Prog. Org. Coatings*, vol. 151, no. February 2021, pp. 106052, 2021, doi: 10.1016/j.porgcoat.2020.106052.

[12]   N. Mohamad *et al.*, "Vibrational damping behaviors of graphene nanoplatelets reinforced NR/EPDM nanocomposites," *J. Mech. Eng. Sci.*, vol.11, no. 4, pp. 3274-3287, 2017, doi: 10.15282/jmes.11.4.2017.28.0294.

[13]   N. Mohamad *et al.*, "Fatigue and mechanical properties of graphene nanoplatelets reinforced NR/EPDM nanocomposites," *J. Phys.: Conf. Series*, vol. 1082, no. 1, pp. 012050(1-6), 2018, https://iopscience.iop.org/article/10.1088/1742-6596/1082/1/012050/pdf.

[14]   T. Kuilla *et al.*, "Recent advances in graphene based polymer composites," *Prog. Poly. Sci.*, vol. 35, no. 11, pp.1350-1375, 2010, doi: 10.1016/j.progpolymsci.2010.07.005.

[15]   P. Jojibabu, Y.X., Zhang, and B. Gangadhara Prusty, "A review of research advances in epoxy-based nanocomposites as adhesive materials," *Int. J. Adhe. Adhes.*, vol. 96, no. January 2020, pp. 102454, 2020, 10.1016/j.ijadhadh.2019.102454.

[16]   Q. Ahsan *et al.*, " Effect of aluminum surface treatment on the damping properties of aluminum-rubber bonding system," In *iMEC-APCOMS 2019. Lecture Notes in Mechanical Engineering*, M. Osman Zahid, R. Abd. Aziz, A. Yusoff, N. Mat Yahya, F. Abdul Aziz, and M. Yazid Abu, Eds. Springer, Singapore, pp. 497-502, 2020, doi: 10.1007/978-981-15-0950-6_76.

[17]   M. Sieradzka, C. Ślusarczyk, R. Fryczkowski, and J. Janicki, "Insight into the effect of graphite grain sizes on the morphology, structure and electrical properties of reduced graphene oxide," *J. Mater. Res. Technol.*, vol. 9, no. 4, pp. 7059-7067, 2020, doi: 10.1016/j.jmrt.2020.05.026.

[18]   I. Ismail, M. K. Harun, and M. Z. A.Yahya, "Effects of dissolved oxygen on the integrity of industrial chlorinated rubber–based primer used in rubber/metal composites," *Rubber Chem. Techno.*, vol. 88, no. 3, pp. 502-514, 2015, doi: 10.5254/rct.15.84905.

[19] H. Alhumade *et al.*, "Enhanced protective properties and UV stability of epoxy/graphene nanocomposite coating on stainless steel," *Express Poly. Lett.*, vol. 10, no. 12, pp.1034-1046, 2016, doi: 10.3144/expresspolymlett.2016.96.

[20] M. Lotfi, H. Yari, M.G. Sari, and A. Azizi, "Fabrication of a highly hard yet tough epoxy nanocomposite coating by incorporating graphene oxide nanosheets dually modified with amino silane coupling agent and hyperbranched polyester-amide," *Prog in Org. Coatings*, vol. 162, pp.106570, 2022, doi: 10.1016/j.porgcoat.2021.106570.

[21] H.J. Yoo, S.S. Mahapatra, and J. W. Cho, "High-speed actuation and mechanical properties of graphene-incorporated shape memory polyurethane nanofibers," *J. Phys. Chem. C*, vol. 118, no. 19, pp. 10408-10415, 2014, doi: 10.1021/jp500709m.

[22] B. Yu *et al.*, "Enhanced thermal and flame retardant properties of flame-retardant-wrapped graphene/epoxy resin nanocomposites," *J. Mater. Chem. A*, vol. 3, no. 15, pp. 8034-8044, 2015, doi: 10.1039/C4TA06613H.

[23] C. Gonçalves *et al.*, "Biocompatible reinforcement of poly(Lactic acid) with graphene nanoplatelets," *Poly. Compos.*, vol. 39, no. S1 Special Issue: Composites for Biological Applications, pp. E308-E320, 2018, doi: 10.1002/pc.24050.

[24] Y. Song *et al.*, "Enhancing the thermal, electrical, and mechanical properties of silicone rubber by addition of graphene nanoplatelets," *Mater. Des.*, vol. 88, pp. 950-957, 2015, doi: 10.1016/j.matdes.2015.09.064.

[25] K.I. Karim *et al.*, "Tensile properties degradation of thermally aged NR/EPDM blend and nanocomposites for engine mounting. *Malaysian J. Compos. Sci. Manuf.*, vol. 2, no. 1, pp. 21–30, 2020, doi: 10.37934/mjcsm.2.1.2130.

[26] P. Jiang *et al.*, "Viscoelastic changes in chlorinated butyl rubber modified with graphene oxide," *Iran Polym. J.*, vol. 26, pp. 861–870, 2017, doi: 10.1007/s13726-017-0570-9.

[27] S. Gunasekaran, R. K. Natarajan, A. Kala, and R. Jagannathan, "Dielectric studies of rubber materials at microwave frequencies," *Indian J. Pure App. Phys.*, vol. 46, pp. 733-737, 2008, doi: http://nopr.niscair.res.in/bitstream/ 123456789/2579/1/IJPAP%2046%2810%29%20733-737.pdf.

[28] G. Xue *et al.*, "Morphology, thermal and mechanical properties of epoxy adhesives containing well-dispersed graphene oxide," *Int. J. Adhe. Adhes.*, vol. 88, pp. 11-18, 2019, doi: 10.1016/j.ijadhadh.2018.10.011.

[29] F.Y. Li *et al.*, "Probing the reinforcing mechanism of graphene and graphene oxide in natural rubber," *J. App. Poly. Sci.*, vol. 129, no. 4, pp. 2342-2351, 2013, doi: 10.1002/app.38958.

[30] H.M. Chong, S.J. Hinder, and A.C. Taylor, "Graphene nanoplatelet-modified epoxy: effect of aspect ratio and surface functionality on mechanical properties and toughening mechanisms," *J. Mater. Sci.*, vol. 51, no. 19, pp. 8764-8790, 2016, doi: 10.1007/s10853-016-0160-9.

[31] Z. Ahmadi, "Nanostructured epoxy adhesives: A review," *Prog. Org. Coatings*, vol. 135, pp. 449-453, 2019, doi: 10.1016/j.porgcoat.2019.06.028.

[32] A. Safari, M. Farahani, and P. Ghabezi, "Experimental study on influences of different surface treatment processes and adhesive type on aluminum adhesive-bonded joint strength," *Mech. Base Des. Struct. Mach.*, pp. 1-14, 2020, doi: 10.1080/15397734.2020.1777876.

[33] A. Liang *et al.*, "Recent developments concerning dispersion methods and mechanisms of graphene," *Coatings*, vol. 8, no. 1, pp. 33, 2018, doi: 10.3390/coatings8010033.